

# **Charge Transfer at Hybrid Interfaces: Plasmonics of Aromatic Thiol-Capped Gold Nanoparticles**

Claire Goldmann,<sup>1</sup> Rémi Lazzari,<sup>2</sup> Xaviez Paquez,<sup>1</sup> Cédric Boissière,<sup>1</sup> François Ribot,<sup>1</sup> Clément Sanchez,<sup>1</sup> Corinne Chanéac<sup>1</sup> and David Portehault<sup>1,\*</sup>

<sup>1</sup> Sorbonne Universités, UPMC Univ Paris 06, CNRS, Collège de France, Laboratoire de Chimie de la Matière Condensée de Paris, 11 place Marcelin Berthelot, F-75005, Paris, France

<sup>2</sup> Sorbonne Universités, CNRS, UPMC Univ Paris 06, Institut des NanoSciences de Paris, 4 Place Jussieu, F-75005, Paris, France

To whom correspondence should be addressed: david.portehault@upmc.fr

## Table of Content

**Figure S1.** Detailed procedures of ligands exchange and titration.

**Figure S2.** TEM pictures and size distributions of nanoparticles before and after exchange with TerPh ligands.

**Figure S3.** NOESY experiments.

**Figure S4.** TEM pictures, size distributions and UV-vis. spectra of nanoparticles derived from Brust's method and synthesized with DDT or TerPh ligands.

**Figure S5.** TEM pictures of nanoparticles derived from Stucky's method, grafted with DDT and after exchange with TerPh, BiPh and Ph ligands.

**Figure S6.** Time evolution of the maximum absorbance at  $\lambda_{\max}$  during exchange of DDT with Ph, BiPh and TerPh.

**Figure S7.** Raw ellipsometric data for the TerPh ligand SAM and fits.

**Figure S8.** Raw ellipsometric data for the DDT ligand SAM and fits.

**Table S1.** Summary of ellipsometric modelization of terphenylthiol and dodecanethiol SAMs.

**Figure S9.** a) Density of charge carriers and b) charge carrier mobility.

**Figure S10.** Dielectric function of the bare gold substrate with no ligand layer, modeled from spectroscopic ellipsometry measurements and simulation of absorbance spectra with and without inter-band transitions terms.

**Table S2.** Parameters obtained from the fit of the reported dielectric function of gold and from the fit of the experimental data reported in Figure S9.

**Figure S11.** Simulation of UV-visible spectra of 5 nm spherical gold nanoparticles without any shell, with varying parameters.

**Figure S12.** Experimental UV-visible spectra obtained for different ligand shell compositions, and fitted spectra by adjusting the contribution of only *s* electrons or both *s* and *d* electrons.

**Figure S13.** Simulation of the experimental absorbance spectra of the grafted particles over the whole spectral range with the fitted parameters of Table 2.

**Table S3.** Reliability factors for fitted spectra shown in figure S11.

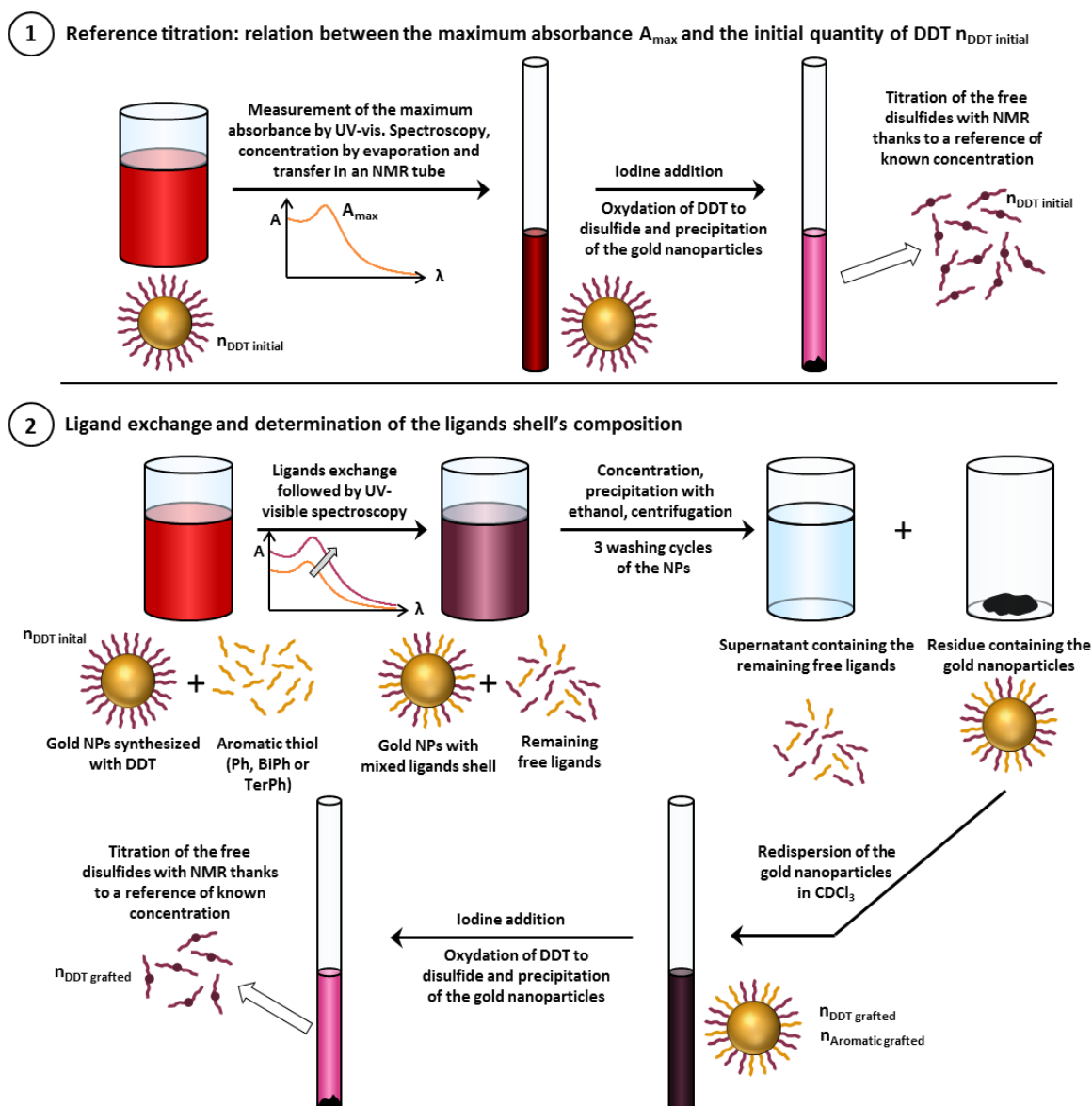


**Figure S1.** Detailed procedures used **(1)** to determine the initial quantity of grafted DDT, and **(2)** to measure the optical properties of the suspensions and evaluate the composition of the ligand shell after exchange.

In point **(1)**, an aliquot of gold nanoparticles covered with DDT and dispersed in a known volume of  $\text{CHCl}_3$  is taken from a given batch and a UV-visible spectrum is acquired to measure  $A_{\max}$ . Then, this same aliquot of nanoparticles is concentrated by evaporation, redispersed in  $\text{CDCl}_3$  and transferred in an NMR tube with no loss. Iodine is added into the tube to oxidize all the DDT molecules into the corresponding disulfides, which are released from the gold surface. Then the NMR spectrum is acquired and compared to a reference tube of known concentration to determinate  $n_{\text{DDT initial}}$ . Experiments show that for different aliquots of the given batch, all the nanoparticles have the same size and grafting density. Thus, point **(1)** allows us to correlate  $A_{\max}$  to  $n_{\text{DDT initial}}$  for each aliquot coming from the same synthesis batch.

Point **(2)** describes the determination of the surface composition. Gold nanoparticles covered with DDT are dispersed in a known volume of  $\text{CHCl}_3$  and  $A_{\text{max}}$  of the sample is measured. Thanks to point **(1)**,  $A_{\text{max}}$  allows the determination of  $n_{\text{DDT initial}}$ . A known quantity of aromatic ligands is then added and the UV-visible spectra are recorded until they reach stability. The reaction medium is then concentrated, the nanoparticles are separated from the supernatant by centrifugation after precipitation with ethanol and they are washed several times to get rid of the free ligands. Then, the particles are redispersed in  $\text{CDCl}_3$  and transferred into an NMR tube with no loss. After iodine addition, the NMR spectrum is acquired and allows the quantification of the grafted DDT at the end of the ligand exchange,  $n_{\text{DDT grafted}}$ . Because iodine reacts with the aromatic groups, the amount of grafted aromatic ligands cannot be directly determined. Knowing the initial quantity of DDT before ligand exchange and because the exchange occurs in a 1:1 stoichiometry, we can determine the final quantity of aromatic ligand grafted on the surface thanks to the relation:

$$n_{\text{Aromatic grafted}} = n_{\text{DDT initial}} - n_{\text{DDT grafted}}$$

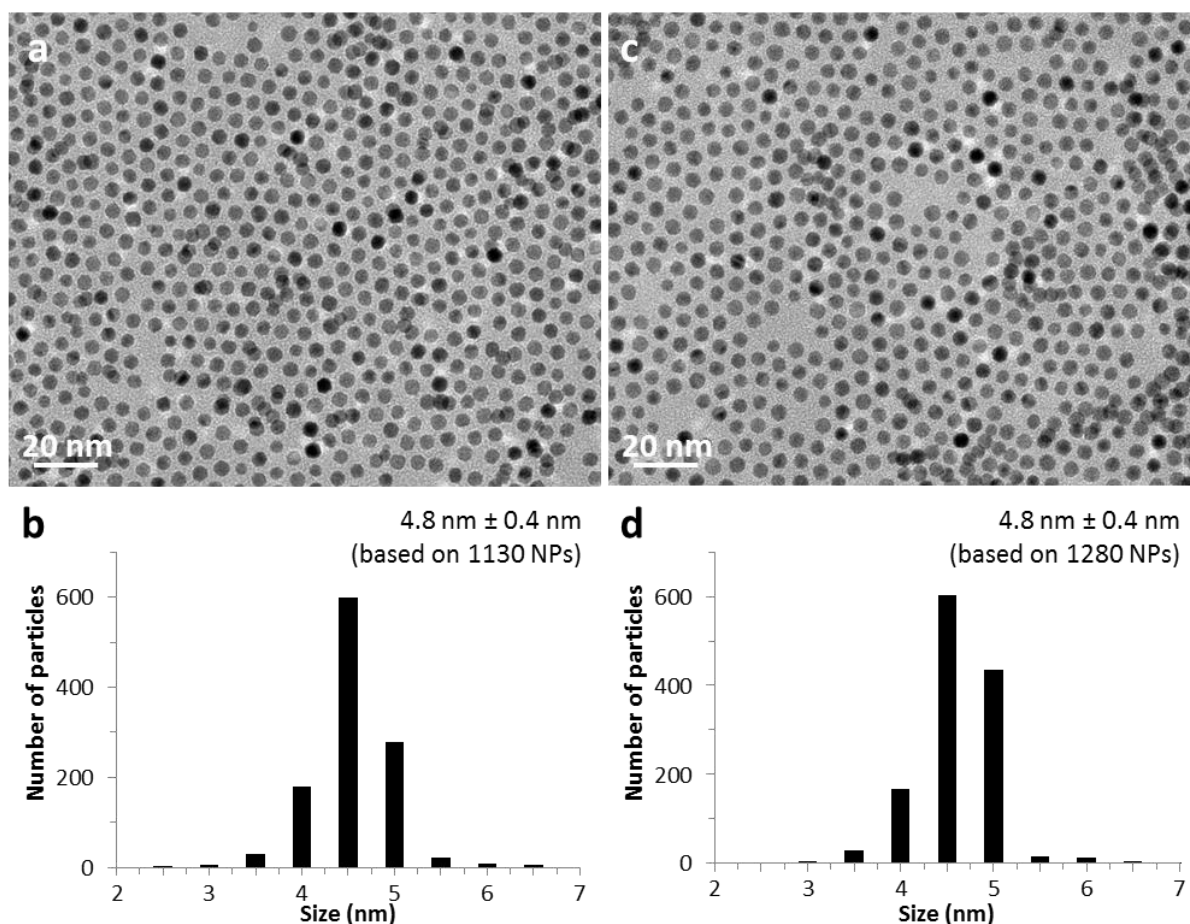


**Figure S2.** a) TEM picture of nanoparticles synthesized with DDT and b) the corresponding size distribution. c) TEM picture of the same particles with 52% of TerPh on the surface after ligand exchange and d) the corresponding size distribution. The size and polydispersity remain unchanged after ligand exchange and the particles are well dispersed on the TEM grid. Accordingly, after ligand exchange for shells containing up to 55 % of aromatic thiol, the particles size and the dispersion state remain unchanged.

Therefore, digestive ripening and concomitant size evolution (Jana, N. R.; Gearheart, L.; Murphy, C. J. Seeding Growth for Size Control of 5–40 Nm Diameter Gold Nanoparticles. *Langmuir* **2001**, *17*, 6782–6786; and Link, S.; El-Sayed, M. a. Size and Temperature Dependence of the Plasmon Absorption of Colloidal Gold Nanoparticles. *J. Phys. Chem. B* **1999**, *103*, 4212–4217) as well as aggregation (Ajzik, A.; Patakfalvi, R.; Hornok, V.; Dékány, I. Growing and Stability of Gold Nanoparticles and Their Functionalization by Cysteine. *Gold Bull.* **2009**, *42*, 113–123; and Wei, Y.; Han, S.; Kim, J.; Soh, S.; Grzybowski, B. a. Photoswitchable Catalysis Mediated by Dynamic Aggregation of Nanoparticles. *J. Am. Chem. Soc.* **2010**, *132*, 11018–11020) can be safely ruled out as causes for the observed red shift.

Noteworthy, as aggregation and ripening are observed for higher contents of ArSH (not shown), the study on 5 nm particles was focused on bi-ligand corona with a composition in aromatic ligand below 55%.

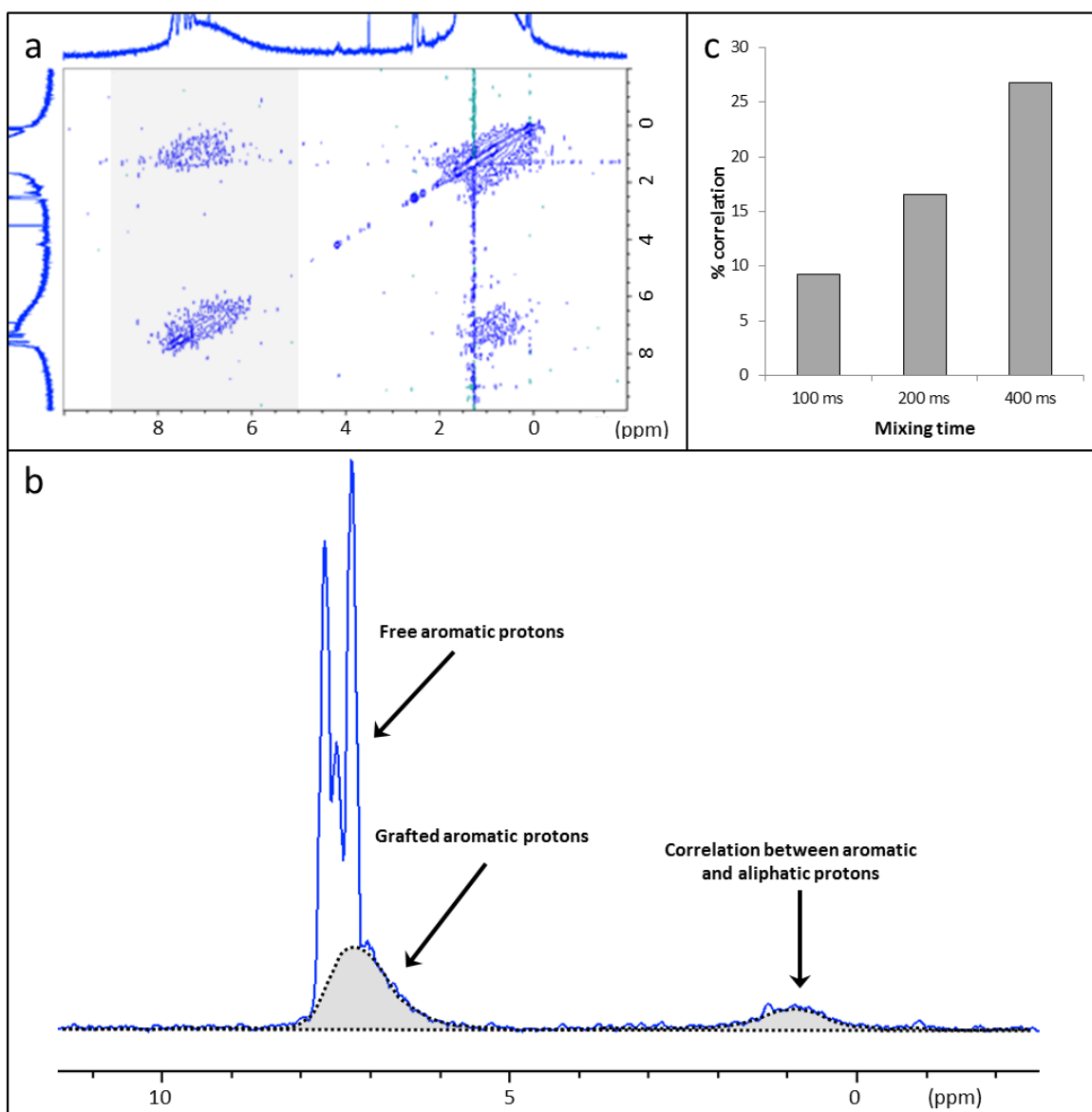


**Figure S3.** **a)** 2D-mapping of a NOESY experiment with a mixing time of 400 ms, done on 5 nm particles with a shell composition DDT:TerPh 50:50. **b)** Positive projection in 1D of the grey zone shown in a). The grafted and bonded aromatic ligands can be easily identified thanks to the peaks width (Kohlmann, O.; Steinmetz, W. E.; Mao, X.; Wuelfing, W. P.; Templeton, A. C.; Murray, R. W.; Johnson, C. S. NMR Diffusion, Relaxation, and Spectroscopic Studies of Water Soluble, Monolayer-Protected Gold Nanoclusters. *J. Phys. Chem. B* **2001**, *105*, 8801-8809). The bonded aromatic protons signal and the correlation peak are fitted with mixed Gaussian/Lorentzian curves and their respective areas are compared. The correlation peak area is normalized with the bonded aromatic protons area. **c)** Normalized intensity of the correlation peak area for different mixing times.

NOESY NMR has already been used in the literature to investigate the phase segregation of the ligands on gold nanoparticles (Liu X.; Yu M.; Kim H.; Mameli M.; Stellacci F. Synthesis and Characterization of Janus Gold Nanoparticles. *Nat. Commun.* **2012**, *3*, 1182). It is known that the mixing time can influence the intensity of the correlation peak (Claridge T. D. W. High-resolution NMR techniques in organic chemistry Second edition; *Tetrahedron Organic*

*Chemistry Series*, **2009**, 27, 1-383) so it is necessary to investigate several ones. Here, whatever the mixing time, a strong correlation peak between aliphatic and aromatic protons is observed, showing that the two kinds of protons are spatially close to each other, thus suggesting homogeneous mixed shells: phase separation of the ligands can be ruled out.

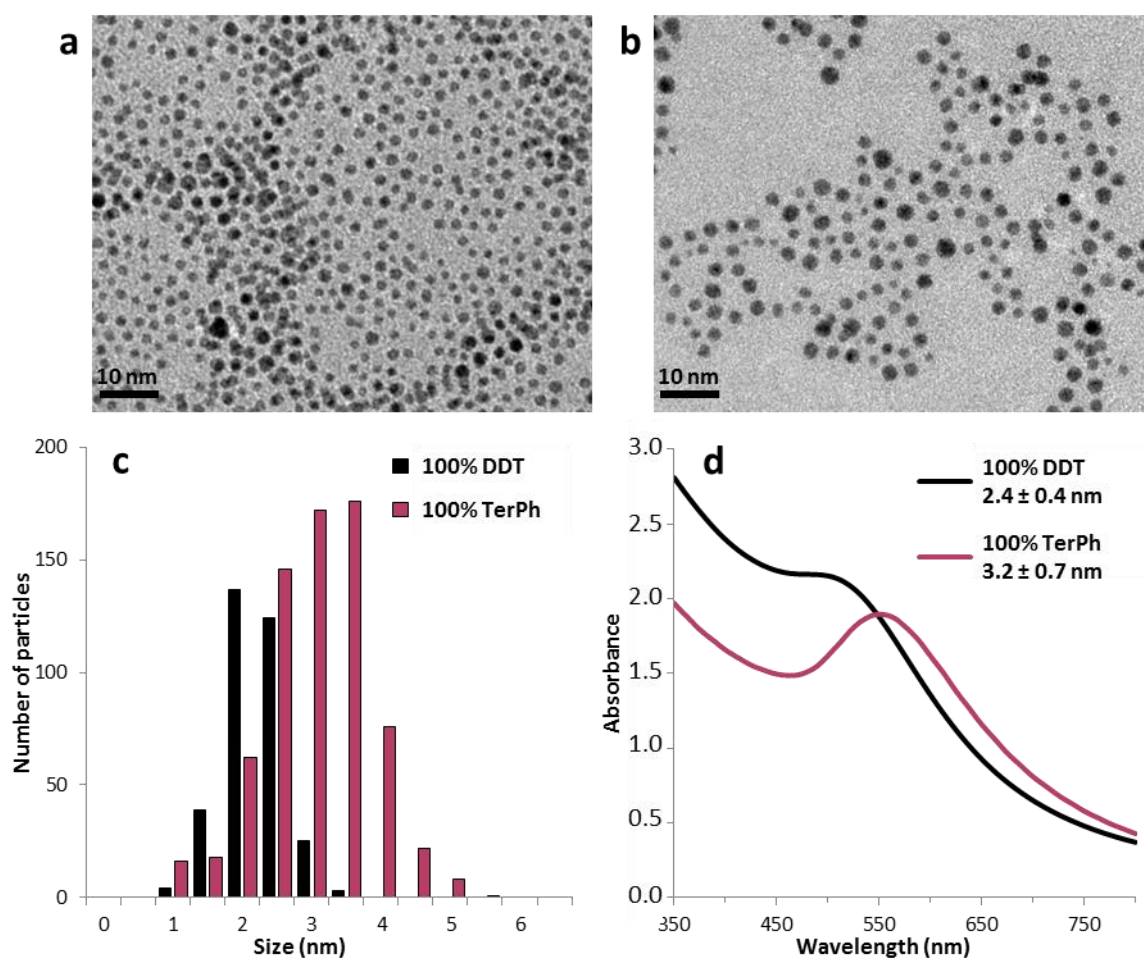


**Figure S4.** TEM picture of ~2-3 nm nanoparticles synthesized by Brust method with **a)** DDT and **b)** TerPh. **c)** UV-visible spectra of the particles suspensions in chloroform. With DDT,  $\lambda_{\max} = 510$  nm, with TerPh,  $\lambda_{\max} = 550$  nm. **d)** Size distribution of the particles.

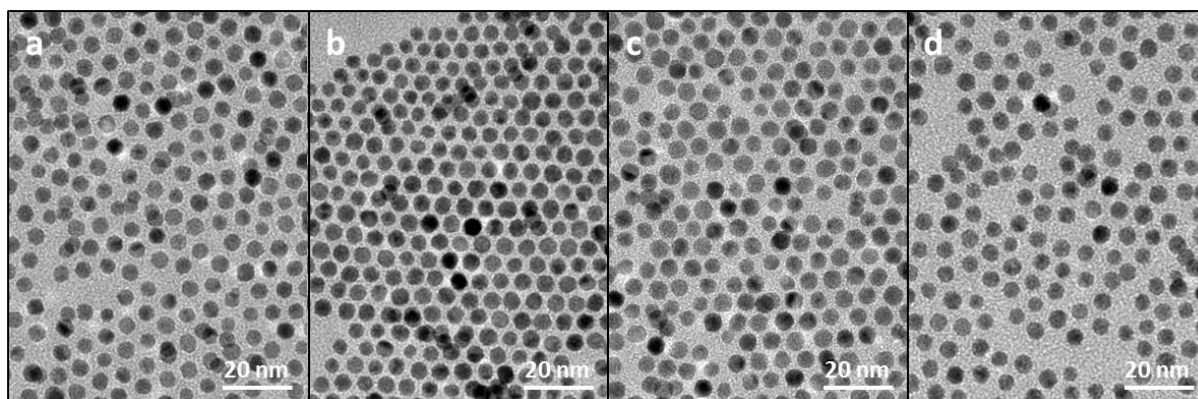


**Figure S5.** TEM picture of nanoparticles **a)** initially synthesized with DDT and a diameter of 5 nm and after completion of ligand exchange with aromatic thiols, reaching the following compositions: **b)** DDT:Ph 59:41 after 48h of exchange, **c)** DDT:BiPh 50:50 after 48h of exchange and **d)** DDT:TerPh 45:55 after 75h of exchange. No size modification neither aggregation is observed.

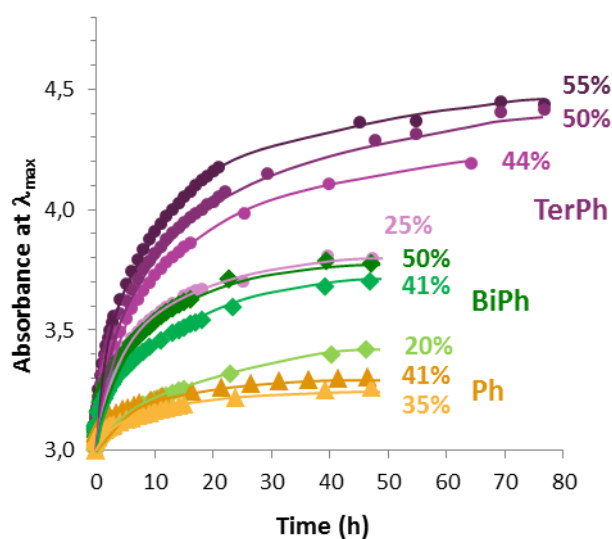


**Figure S6.** Time evolution of the maximum absorbance at  $\lambda_{\max}$  during exchange of DDT with Ph, BiPh and TerPh. The indicated percentage is the final proportion of the aromatic ligand on the gold nanoparticles surface.



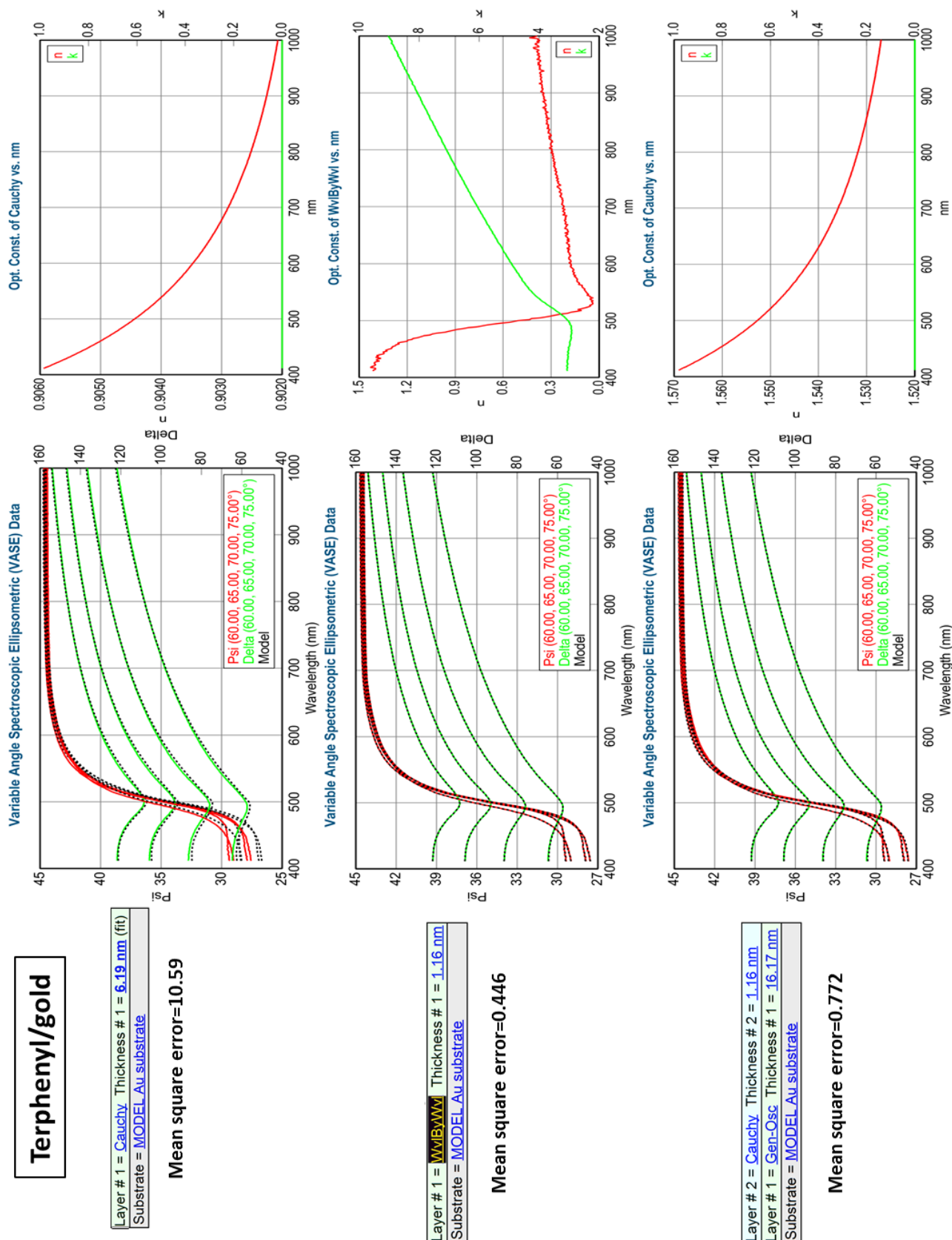


**Figure S7.** Raw ellipsometric data for the TerPh ligand SAM and fits with (top) only two layers with Cauchy description of the organic layer, (middle) only 2 layers with a Wavelength by wavelength model, (down) a 3 layer model. Interpretation in Table S1.

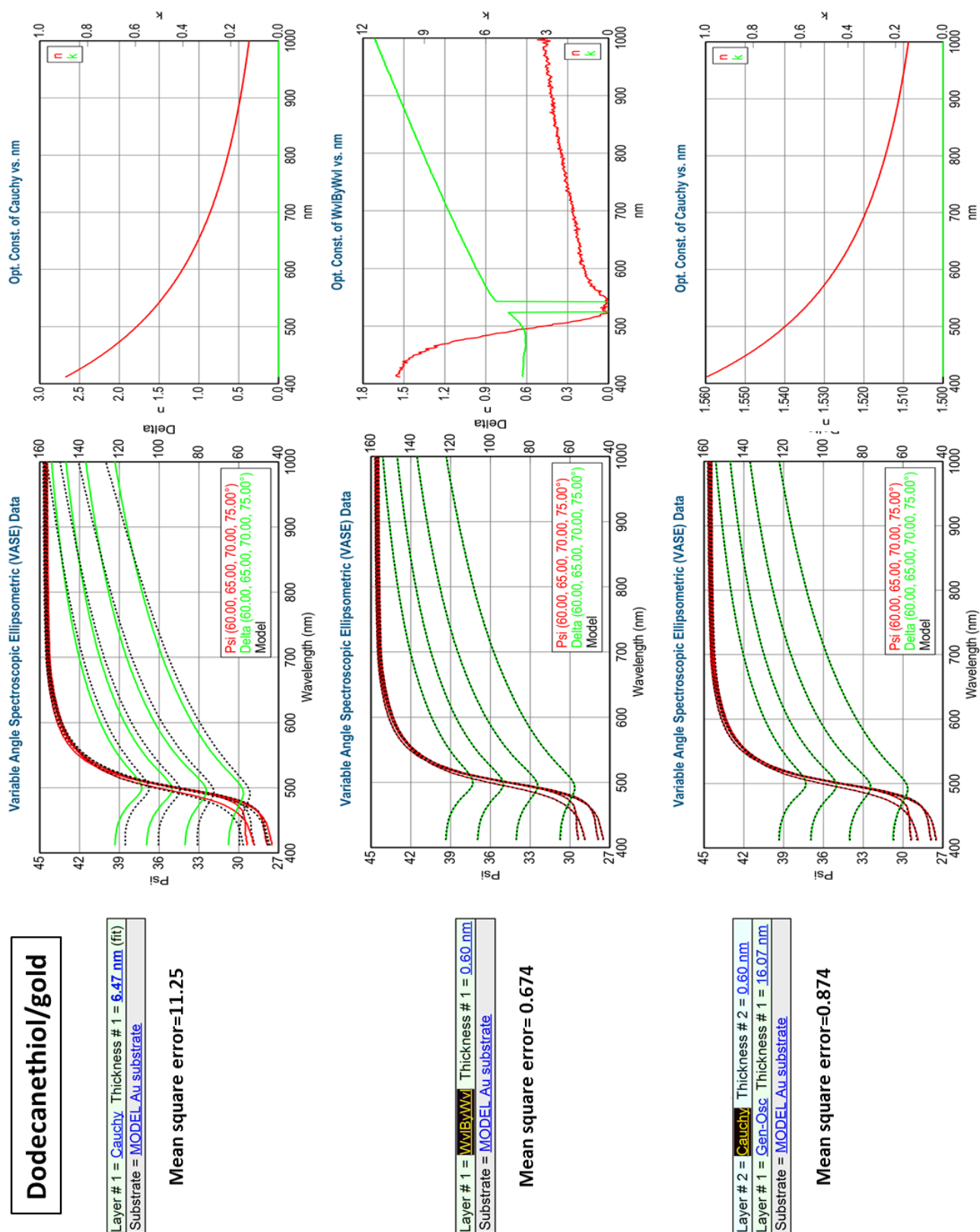


**Figure S8.** Raw ellipsometric data for the DDT ligand SAM and fits with (top) only two layers with Cauchy description of the organic layer, (middle) only 2 layers with a Wavelength by wavelength model, (down) a 3 layer model. Interpretation in Table S1.

**Table S1.** Summary of ellipsometric modeling (Figures S6 and S7) of terphenylthiol and dodecanethiol SAMs.

SAM composition	Model	Fit quality	SAM thickness	SAM Optical properties
Terphenylthiol	<u>Dielectric</u> Gold substrate	Bad	Unrealistic	Unrealistic
Terphenylthiol	<u>Wvl by Wvl</u> Gold substrate	Good	Good	Unrealistic
Terphenylthiol	<u>Dielectric</u> <u>Modified gold</u> Gold substrate	Good	Good	Good
Dodecanethiol	<u>Dielectric</u> Gold substrate	Bad	Unrealistic	Unrealistic
Dodecanethiol	<u>Wvl by Wvl</u> Gold substrate	Good	Good	Unrealistic
Dodecanethiol	<u>Dielectric</u> <u>Modified gold</u> Gold substrate	Good	Good	Good

Ellipsometric modeling using two optical layers either fail describing experimental data or release unrealistic description of SAMs layers. In such a case, optical properties of SAM layer are unrealistic and/or SAM thickness is beyond the maximum length of the fully extended SAM molecule). The direct inversion of SAMs optical properties from a Wavelength-by-wavelength model indicates that the SAM/gold substrate stack presents metallic properties different from that of bare gold substrate.

By adding an intermediate layer (in between SAM and gold substrate) with metallic properties, both optical properties and thickness of SAMs layers obtained by modelling are physically realistic and coherent with data of the literature. Only these experimental SAMs data (optical dispersion of SAMs layers  $n=F(\text{wavelength})$  and thicknesses) were used for modelling UV-Vis experiments.

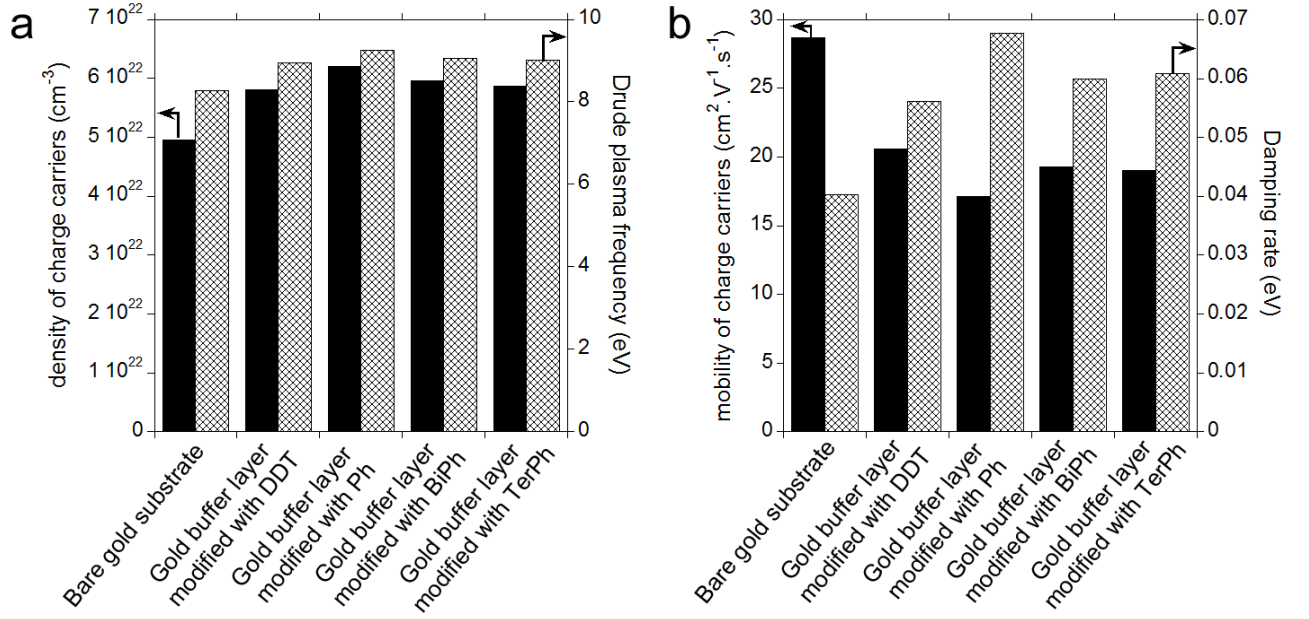


**Figure S9.** **a)** Density of charge carriers, corresponding Drude plasma frequency (from equation (4) in the main text  $\omega_D = \sqrt{\frac{n_s e^2}{m_e \epsilon_0}}$ ), **b)** charge carrier mobility and corresponding damping rate  $\Gamma_D$  in the bare gold substrate and gold buffer layers modified with each ligand. These data are calculated from the free-electron Drude model applied to ellipsometry measurements, where

$$\epsilon_{DRUDE}(E) = \frac{-\hbar^2 \cdot q^2 \cdot n_s \cdot \mu}{\epsilon_0 (\mu \cdot m_e \cdot E^2 - i \cdot q \cdot E \cdot \hbar)}$$

Corresponds to the first 2 parts of equation (3) in the main text:

$$\epsilon_g(\omega) = \epsilon_\infty - \frac{\omega_D^2}{\omega^2 - i\omega\Gamma_D} + G_1(\omega) + G_2(\omega) \quad (3)$$

With  $\hbar$  the Planck constant/ $2\pi$ ,  $q$  the electron charge,  $n_s$  the carrier concentration in  $\text{cm}^{-3}$ ,  $\mu$  the carrier mobility in  $\text{cm}^2 \text{V}^{-1} \text{s}^{-1}$ ,  $\epsilon_0$  the vacuum dielectric constant and  $m_e$  is the electron rest mass.

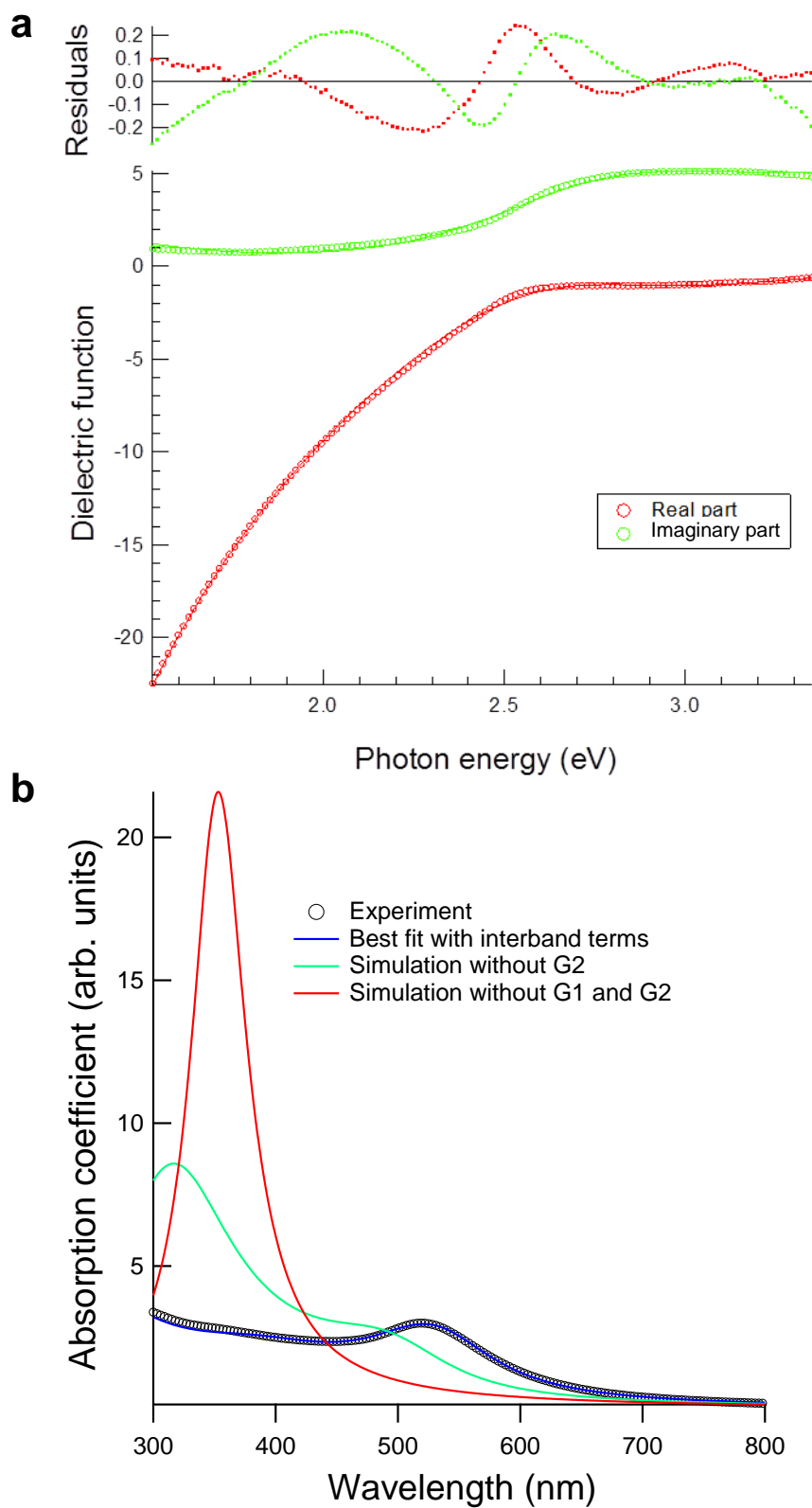


**Figure S10.** (a) Dielectric function of the bare gold substrate (symbols) with no ligand layer, modeled from spectroscopic ellipsometry measurements and expression (3) (main text). (b) Simulation of absorbance spectra with and without inter-band transitions terms  $G_1(\omega)$  and  $G_2(\omega)$ . Parameters correspond to those of the best fits of DDT spectrum (circles) (Figure 7a).

**Table S2.** Parameters obtained <sup>a</sup> from the fit detailed in Etchegoin (ref. 44 Etchegoin, P. G.; Le Ru, E. C.; Meyer, M. An Analytic Model for the Optical Properties of Gold. J. Chem. Phys. 2006, 125, 1–4) of the dielectric function of gold reported in ref 36 and <sup>b</sup> from the fit of the experimental data reported in Figure S10.

	Fit range	$\epsilon_\infty$	$\hbar\omega_D$ (eV)	$\hbar\Gamma_D$ (eV)	$\hbar C_1$ (eV)	$\phi_1$ (°)	$\hbar\omega_1$ (eV)	$\hbar\Gamma_1$ (eV)	$\mu_1$	$\hbar C_2$ (eV)	$\phi_2$ (°)	$\hbar\omega_2$ (eV)	$\hbar\Gamma_2$ (eV)	$\mu_2$
Fit of (n,k) <sup>a</sup>	1.2 – 6.2 eV	1.53	8.5506	0.0729	2.49	-45	2.6490	0.5390	1	5.093	-45	3.745	1.319	1
Fit of ( $\epsilon_1$ , $\epsilon_2$ ) Data of bulk gold Au(111) <sup>bc</sup>	1.2 – 3.3 eV	1.49	8.218	0.0818	2.287	-45	2.6650	0.5400	1	4.963	-45	3.779	1.261	1

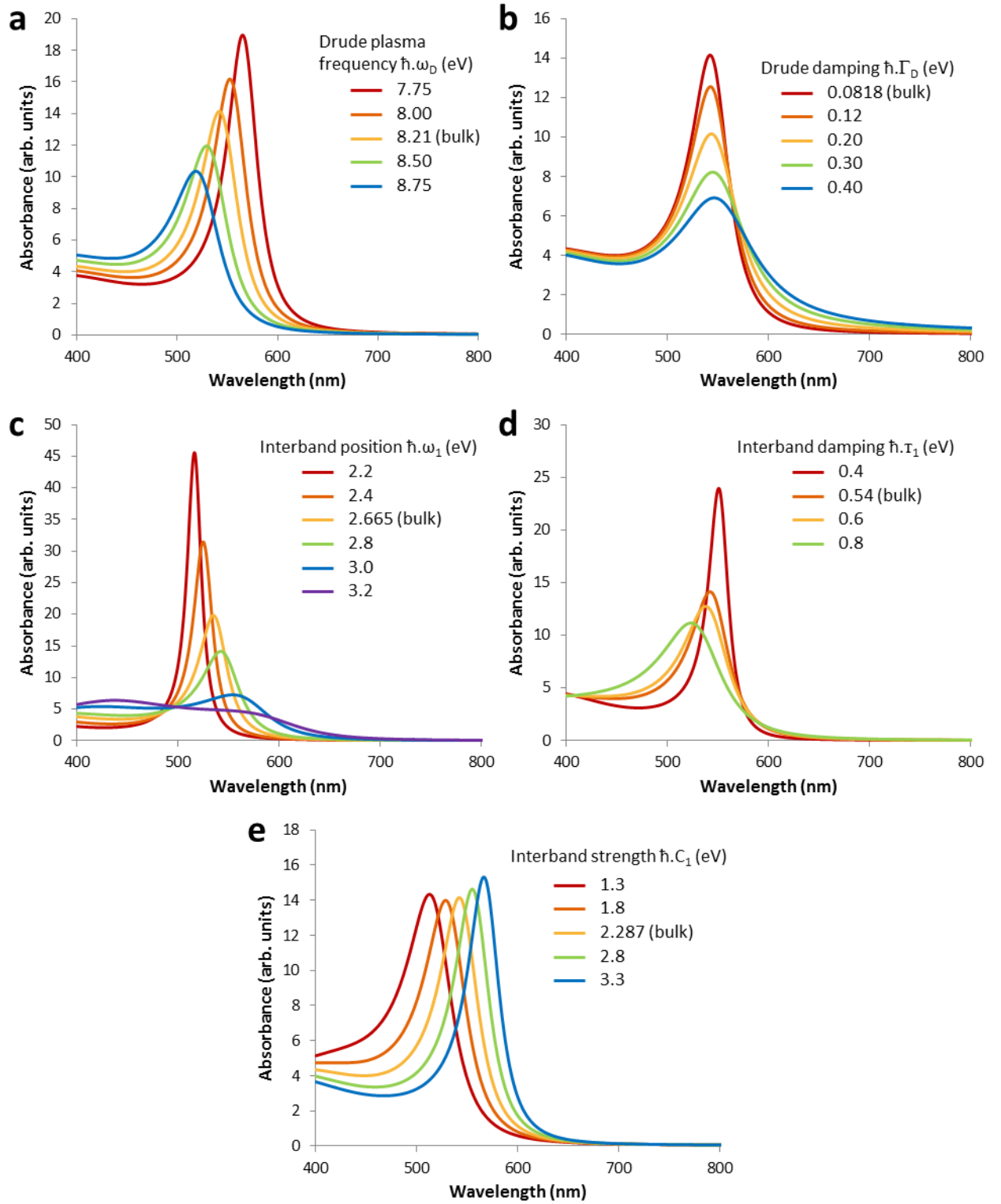


**Figure S11.** Simulation of UV-visible spectra of 5 nm spherical gold nanoparticles without any shell, with varying parameters a)  $\hbar\omega_D$ , b)  $\hbar\Gamma_D$ , c)  $\hbar\omega_1$ , d)  $\hbar\Gamma_1$  and e)  $\hbar C_1$ . Values are chosen around the bulk ones.

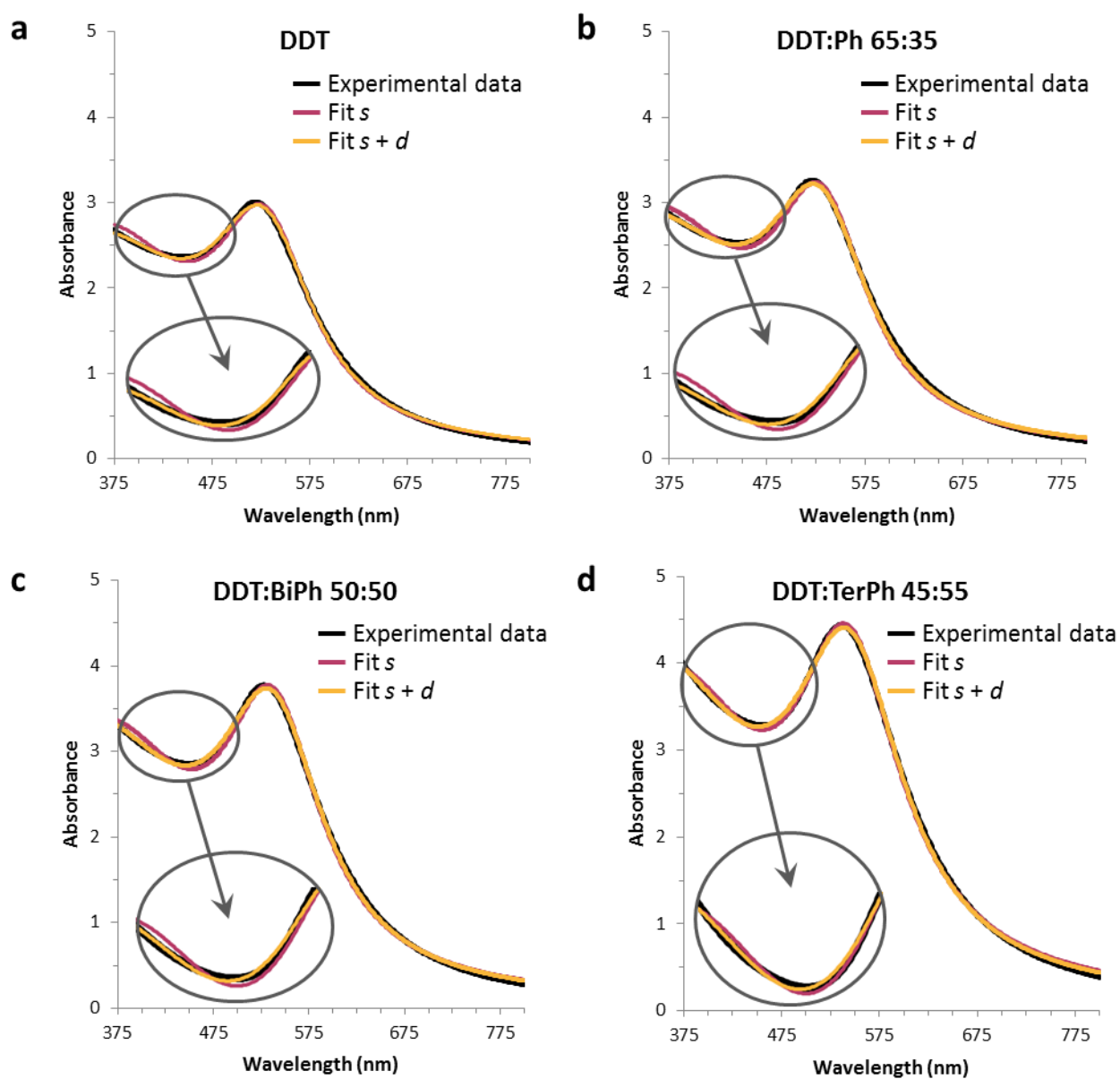


**Figure S12.** Experimental UV-visible spectra obtained for different ligand shell compositions, and fitted spectra by adjusting the contribution of only  $s$  electrons (Drude model) or both  $s$  and  $d$  electrons (Drude model and interband transitions).



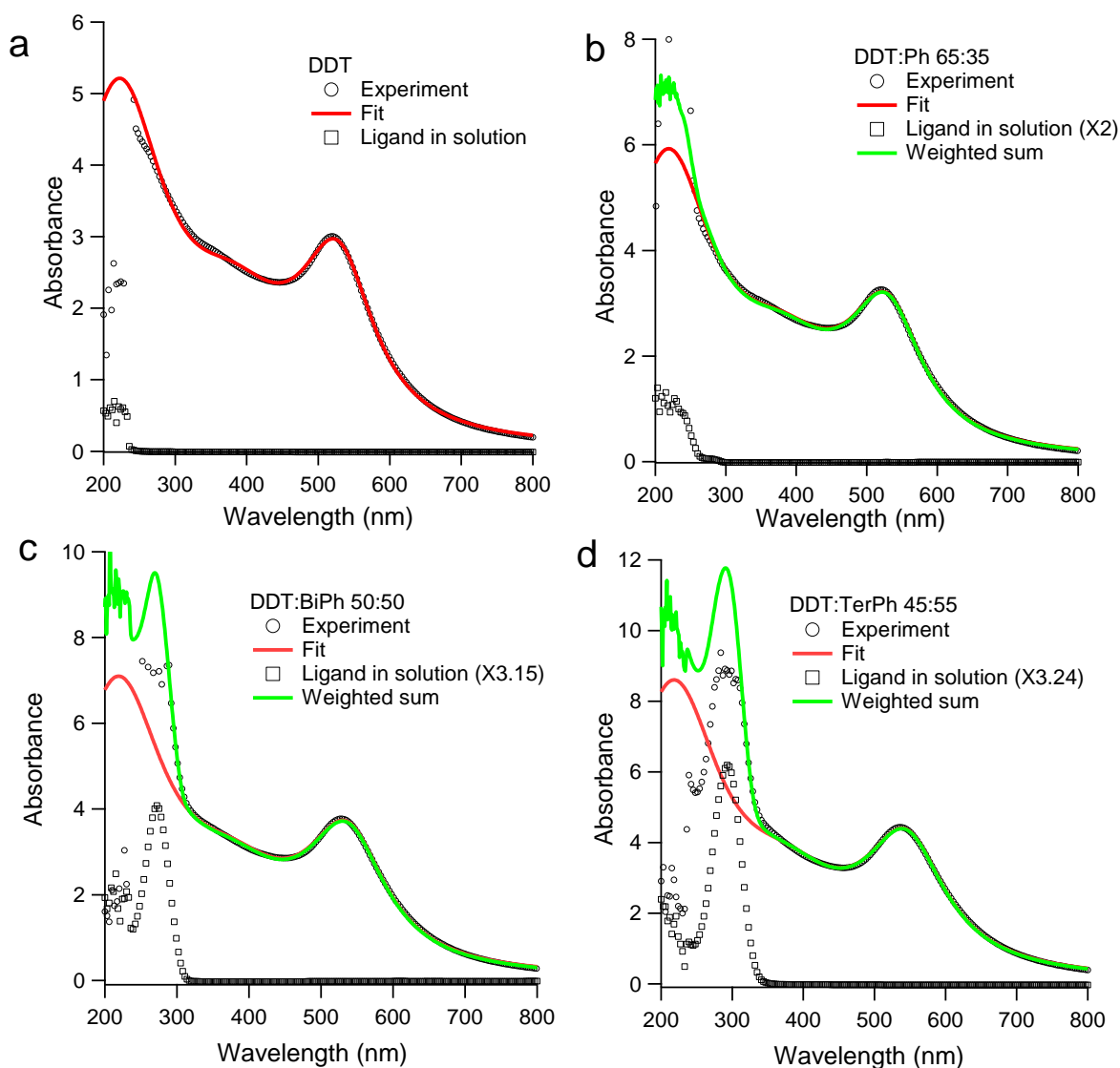


**Figure S13.** Simulation (red line) of the experimental absorbance spectra (open circles) of the grafted particles over the whole spectral range with the fitted parameters of Table 2. A better agreement (green line) is obtained by adding the absorbance of the molecules alone in solution (open square). The weighting prefactor is given by the ratio of concentration. Notice that above 8, the experimental absorbance is not reliable because of the limited sensitivity of the spectrometer.

**Table S3.** Reliability factors of fitted spectra shown in figure S12. Definitions of  $\chi^2$  and  $R_B$  are shown below.

<b>Ligand shell</b>	<b><math>\chi^2 \times 10^4</math> (fit s)</b>	<b><math>R_B</math> (fit s)</b>	<b><math>\chi^2 \times 10^4</math> (fit s+d)</b>	<b><math>R_B</math> (fit s+d)</b>
<b>DDT</b>	17.65	2.27%	3.90	1.13%
<b>Ph:DDT 35:65</b>	22.99	2.44%	5.69	1.25%
<b>BiPh:DDT 50:50</b>	23.02	2.12%	7.48	1.18%
<b>TerPh:DDT 55:45</b>	17.50	1.49%	9.26	1.09%

$$\chi^2 = \frac{1}{N} \sum_{i=1}^N (y_i^{obs} - y_i^{calc})^2$$

$$R_B = \sum_{i=1}^N |y_i^{obs} - y_i^{calc}| / \sum_{i=1}^N |y_i^{obs}|$$